Aerosol Science and Technology
Publication details, including instructions for authors and subscription information:
http://www.tandfonline.com/loi/uast20

Large Particle Penetration During PM_{10} Sampling

William B. Faulkner[a], Raleigh Smith[a] & John Haglund[b]
[a] Department of Biological and Agricultural Engineering, Texas A&M University, Texas, USA
[b] Department of Mechanical Engineering, Texas A&M University, Texas, USA
Accepted author version posted online: 17 Apr 2014.Published online: 19 May 2014.

Aerosol Science and Technology, 48:676–687, 2014

ISSN: 0278-6826 print / 1521-7388 online
DOI: 10.1080/02786826.2014.915005

Large Particle Penetration During PM_{10} Sampling

William B. Faulkner,[1] Raleigh Smith,[1] and John Haglund[2]
[1]*Department of Biological and Agricultural Engineering, Texas A&M University, Texas, USA*
[2]*Department of Mechanical Engineering, Texas A&M University, Texas, USA*

The objective of the present study was to characterize the performance of a federal reference method (FRM) PM_{10} size-selective inlet using analysis methods designed to minimize uncertainty in measured sampling efficiencies for large particles such as those most often emitted from agricultural operations. The performance of an FRM PM_{10} inlet was characterized in a wind tunnel at a wind speed of 8 km/h. Data were also collected for 20 and 25 μm particles at wind speeds of 2 and 24 km/h. Results of the present sampler evaluation compared well with those of previous studies for a similar inlet near the cutpoint, and the sampler passed the criteria required for certification as a FRM sampler when tested at 8 km/h. Sampling effectiveness values for particles with nominal diameters of 20 and 25 μm exceeded 3% for 8 and 24 km/h wind speeds in the present study and were statistically higher than both the "ideal" PM_{10} sampler (as defined in 40 CFR 53) and the ISO (1995) standard definition of thoracic particles ($p < 0.05$) for 25 μm particles leading to the potential for significant sampling bias relative to the "ideal" PM_{10} sampler when measuring large aerosols.

INTRODUCTION

Exposure to high concentrations of thoracic aerosols has been linked to significant, negative health effects, including increased incidence of asthma, cardiovascular disease, mortality, and morbidity. The National Ambient Air Quality Standards (NAAQS) were established to protect public health and welfare by limiting the concentrations of ambient pollutants to which the public is exposed. The NAAQS for PM_{10} is intended to protect the public against high concentrations of thoracic particles. Compliance with the NAAQS is demonstrated through use of ambient particulate matter (PM) monitors that measure 24-h integrated concentrations of pollutants. Special-use monitors may also be placed at or near the property lines of some sources to ensure that emissions from that source do not lead to public exposure to concentrations exceeding the NAAQS.

When monitoring PM_{10} concentrations for regulatory purposes, it is important that measured concentrations of PM_{10} are representative of concentrations of particles that have the potential to cause adverse health effects. PM_{10} samplers are designed to allow those particles expected to penetrate past the larynx of the human respiratory system to penetrate the sampler precollector and deposit on a filter. The American Conference of Governmental Industrial Hygienists (ACGIH) has defined the "thoracic fraction" of particles, and that definition has been adopted as a standard by International Standards Organization (Figure 1; ISO 1995).

In the Code of Federal Regulations (CFR), the U.S. Environmental Protection Agency (USEPA) has defined the performance of an "ideal" PM_{10} sampler (Figure 1; 40 CFR 53.43) that "approximates the penetration of particles into the human respiratory tract" (40 CFR 53.40(d)). The fractional penetration, or sampling efficiency, of the "ideal" PM_{10} sampler closely matches that of the ACGIH/ISO curve for particles 13 μm in diameter and smaller, but substantial differences in penetration efficiency can be seen for particles between 14 and 27 μm.

For a new PM_{10} sampler to be designated as Federal Reference Method (FRM) or Federal Equivalent Method (FEM) sampler, the sampling effectiveness of the candidate sampler must be compared to the "ideal" PM_{10} sampler. This process requires four general steps specified in 40 CFR 53 Subpart D:

(1) The sampling effectiveness of the candidate inlet is tested in a wind tunnel using ten specific monodisperse, liquid particle sizes ranging from 3 ± 0.5 to 25 ± 1.0 μm in aerodynamic diameter (AD) at wind speeds of 2, 8, and 24 km/h.
(2) For each wind speed, the sampling effectiveness curve of the candidate sampler is determined by fitting a smooth curve to the test data and extrapolating the upper and lower ends of the curve to 100% effectiveness for 1.0 μm AD particles and 0% effectiveness for 50 μm AD particles.

Received 30 January 2014; accepted 8 April 2014.
Address correspondence to William B. Faulkner, Department of Biological and Agricultural Engineering, Texas A&M University, 2117 TAMU, Scoates Hall, College Station, TX 77843, USA. E-mail: Faulkner@tamu.edu
Color versions of one or more of the figures in the article can be found online at www.tandfonline.com/uast.

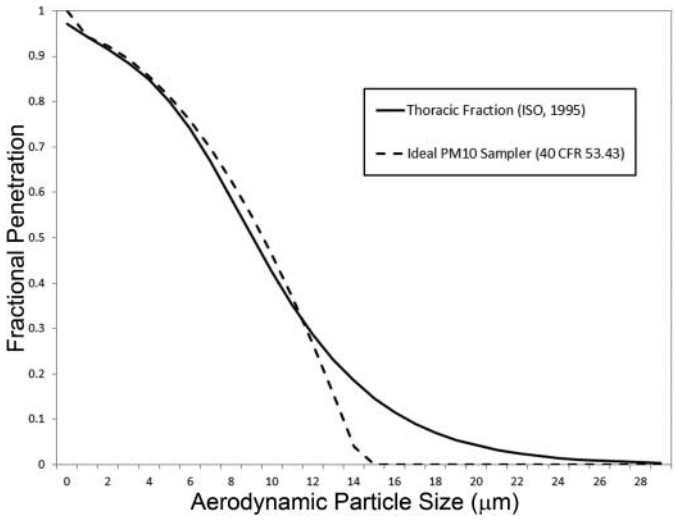

FIG. 1. Fractional penetration for thoracic aerosol fraction (ISO 1995) and "Ideal" PM_{10} sampler (40 CFR 53.43).

(3) The cutpoint of the sampler (i.e., point of 50% sampling effectiveness) is determined. The cutpoint must fall within 10 ± 0.5 μm.
(4) The expected mass concentration that would be collected by the candidate sampler when challenged by a specific polydisperse aerosol whose concentration and particle size distribution (PSD) is given in 40 CFR 53 Table D-3 is calculated and compared to the expected mass concentration that would be collected by the "ideal" PM_{10} sampler, as defined in 40 CFR 53.43. The expected mass concentration that would be collected by the candidate sampler must be within 10% of the concentration that would be collected by the "ideal" sampler (40 CFR 53 Table D-1).

In addition to the liquid particle sampling effectiveness test, candidate samplers must meet the criteria for solid particle sampling effectiveness, measurement precision, and flow rate stability (40 CFR 53 Table D-1).

Researchers involved in sampling of coarse aerosols such as those derived from agricultural and mining sources have reported "oversampling" of PM_{10} concentrations when using FRM PM_{10} inlets compared to concentrations of PM_{10} calculated by applying a theoretical PM_{10} sampling efficiency curve to total suspended particulate samples that were analyzed for PSD (Buser et al. 2008). Aerosols derived from agricultural operations are often primary particles (as opposed to secondary particles formed through atmospheric chemical reactions) and are characterized by larger particle sizes than typical urban aerosols (Table 1).

Despite observations of "oversampling," there is not universal agreement whether the results constitute an "oversampling bias" for industries in which generated particulates typically exhibit a significant coarse fraction. Some experts have argued that ambient particle compositions cannot be reconstructed using the techniques employed by Buser et al. (2008) and others. Furthermore, impactor performance in the precollector of FRM PM_{10} samplers is principally determined by the Stoke's number (Stk, Equation (1)), which should not change for a particle of a given size, regardless of the distribution of particle sizes in an aerosol (i.e., there should be no change in the performance of the sampler as a function of the PSD of the ambient aerosol). However, anecdotal evidence, such as that observed by Buser et al. (2008), suggests that particles much larger than the sampler cutpoint are often observed on the surface of PM sample filters.

$$\mathrm{Stk} = \frac{\tau U}{D_j/2} = \frac{\rho_p d_p^2 U C_c}{9\eta D_j}, \qquad [1]$$

where: τ = particle relaxation time, U = gas velocity, D_j = impactor jet diameter, ρ_p = particle density, d_p = particle diameter C_c = Cunningham's correction factor, and η = gas viscosity.

The objective of the present study was to characterize the performance of a FRM PM_{10} size-selective inlet using analysis

TABLE 1
Lognormal parameters ambient aerosols

Aerosol source	MMD[a] (μm AED)	GSD[b]	Reference
Urban (trimodal) *Nucleation* (0.63 $\mu m^3/cm^3$)	0.038	1.8	USEPA (1996)[c]
Accumulation (38.40 $\mu m^3/cm^3$)	0.32	2.16	
Coarse (30.8 $\mu m^3/cm^3$)	5.7	2.25	
Feedyard	20	2.2	Capareda et al. (2004)
Broiler housing	24	1.6	Lacey et al. (2003)
Dairy	15	2.1	Capareda et al. (2004)
Cotton gin	23	1.8	Wang et al. (2002)

[a]MMD = mass median diameter.
[b]GSD = geometric standard deviation.
[c]USEPA cites Whitby and Sverdup (1980) as the source of lognormal parameters for urban ambient aerosols.

methods designed to minimize uncertainty in measured sampling efficiencies for large particles through the FRM PM_{10} precollector in hopes of facilitating resolution to issues associated with sampling of large particles such as those most often emitted from agricultural operations.

Previous studies have characterized the performance of PM_{10} inlets across a wide range of particle sizes, including particles up to 25 μm AED (McFarland and Ortiz 1984; VanOsdell and Chen 1990; Tolocka et al. 2001). However, analysis methods used in previous studies may not have been optimized to detect the small sampling efficiencies expected when challenging inlets with large particles. For example, fluorometric analysis methods used by McFarland and Ortiz (1984), which will be discussed in detail below, likely masked small sampling efficiency values when characterizing the performance of the original FRM PM_{10} for large particles. Relatively small changes in sampling efficiencies for large particles may not lead to significant changes in collected mass when sampling in urban environments characterized by small particles, but in the presence of large particles, these small values may lead to significant differences in the mass of PM_{10} sampled.

METHODS

The performance of an SA246 PM_{10} inlet (SSI2.5, BGI Inc, Waltham, MA, USA) was characterized in a wind tunnel at a wind speed of 8 km/h. Data were also collected for 20 and 25 μm particles at wind speeds of 2 and 24 km/h. The present study employed methods specifically designed to reduce uncertainties in measured sampling effectiveness values for large particles, including the use of "background control" tests to account for measurement bias introduced by fluorescent contamination of the candidate or isokinetic samplers used and increasing sampler test times to ensure sufficient signal-to-noise ratios during fluorometric analysis of sampler performance. Both of these methods are discussed in greater detail below.

Wind Tunnel Design

Wind tunnels to be used for the evaluation of PM_{10} inlets are required to meet specific criteria outlined in 40 CFR Part 53, Subpart D (henceforth "Subpart D"). The wind tunnel used for the present tests was originally fabricated in the early 1980s for the development and evaluation of PM_{10} inlets (McFarland and Ortiz 1982, 1984). The wind tunnel has been reassembled in order to resume Subpart D testing and evaluation. The 0.61 $\times$ 0.61 meter (2 $\times$ 2 foot) square wind tunnel is comprised of three sections, each 1.22 meters (4 feet) in length, a HEPA filter doubling as a laminar flow device, a flow straightener, a sterman disk, and a flared inlet (Figure 2).

One of the sections (henceforth known as the "test section"; item 5 of Figure 2) has several access ports and windows for testing of sampler inlets. Air is drawn into the wind tunnel by a centrifugal blower (18ACF; New York Blower; Willowbrook, IL, USA) that is controlled with a variable frequency motor controller (VS1PF27-1; Baldor Drives; Fort Smith, AR, USA). Airflow is drawn through a laminar flow device upstream of the test section to straighten the flow and reduce twisting of the streamlines that might be present.

Velocity Profile

An anemometer (VelociCalc 8386, TSI, Inc., Shoreview, MN, USA; accuracy: the greater of $\pm$3.0% or $\pm$0.015 m/s) was used to measure air velocity in the wind tunnel across 33 measurement points (11 points spaced in 50.8 mm (2 inch)

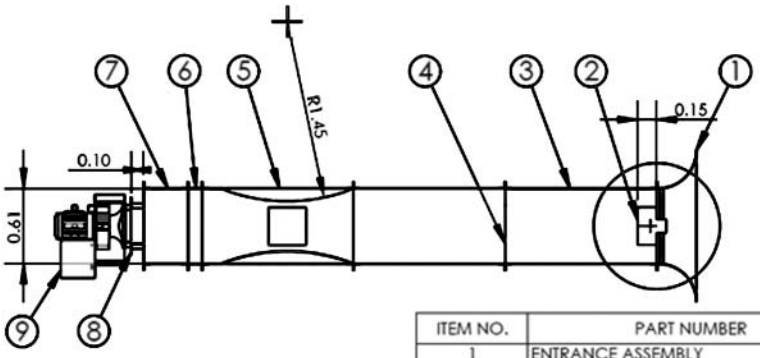

ITEM NO.	PART NUMBER	QTY.
1	ENTRANCE ASSEMBLY	1
2	STERMAN DISK	1
3	TUNNEL SECTION	2
4	AIR STRAIGHTENER	1
5	CURVED TUNNEL SECTION	1
6	HEPA FILTER HOLDER	1
7	TUNNEL SHORT SECTION	1
8	FAN DUCT	1
9	BLOWER	1

FIG. 2. Schematic of the wind tunnel used for testing.

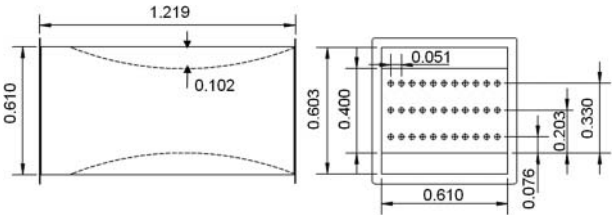

FIG. 3. Velocity measurement sampling grid; dimensions shown are in meters.

intervals at three heights in the sampling plane). In order to achieve an air velocity of 24 km/h, curved 101.6 mm (4 inch) high panels were installed on the roof and the base of the test section of the wind tunnel. These panels remained installed for tests conducted at 2 and 8 km/h as well. Measurements were conducted at 76.2, 203.2, and 330.2 mm (3, 8, and 13 inches) above the raised base of the wind tunnel (Figure 3). The anemometer was programmed to sample at a rate of 1 Hz for a total of 15 s. After 15 s of sampling, the measurements were averaged and recorded. This was repeated at least 11 times per measurement point for a minimum of 396 wind speed measurements across the test section of the wind tunnel for each wind speed.

The longitudinal turbulence intensity describes the degree of turbulence of the airflow in the direction of the airflow. The turbulence intensity value, I, is calculated as the percentage of turbulent flow using Equation (2):

$$I = \frac{w}{U}, \qquad [2]$$

where: u' = standard deviation of the flow measurements at each point U = average wind speed measured at each point.

Average wind speeds for each nominal speed are shown in Table 2. All criteria for wind speed required by 40 CFR 53.42 (e) were satisfied in the TAMU wind tunnel.

Aerosol Generation

Test aerosols were generated with a vibrating orifice aerosol generator (VOAG; Model 3450, TSI, Inc., Shoreview, MN, USA) using specifically constructed solutions for each particle size to produce either liquid (fluorescently tagged oleic acid diluted in ethanol) or solid (ammonium fluorescein diluted in DI water), monodispersed particles. Solutions were constructed to produce a desired particle size based on Equations (3)–(6), adopted from the VOAG user manual and the original VOAG development work by Berglund and Liu (1973). For all tests, liquid aerosol solutions were metered to the VOAG at 0.225 mL/min using a positive displacement, constant flow rate HPLC pump (Series 1500; ChromTech; Apple Valley, MN, USA), and the VOAG vibration frequency was set at a nominal 57,000 Hz (frequencies were adjusted during some tests, as needed, to minimize formation of satellite droplets).

TABLE 2
Velocity uniformity test results

Nominal wind speed (km/h)	Mean wind speed (km/h)	COV (%)	Max std. deviation	Max turbulence intensity (%)
2[a]	2.05	2.29	4.34	3.96
8	8.05	1.32	7.83	1.79
24	24.2	0.47	9.73	0.74

[a]Measured without panels installed.

$$Dp_p = \left(\frac{6 * Q * C}{\pi * f}\right)^{1/3}, \qquad [3]$$

where: Dp_p = physical particle diameter (μm), Q = solution flow rate (mL/s), C = volumetric concentration of aerosol material in the solution (dimensionless), and f = VOAG frequency (Hz).

For liquid aerosols, uranine (CAS 518-47-8) was used as the fluorometric tracer and was combined with oleic acid. This was mixed with an appropriate volume of ethanol to produce the final solution. The concentration of aerosol material for liquid particles was determined as:

$$C_{\text{liq}} = \frac{\frac{m_u}{\rho_u} + \frac{m_o}{\rho_o}}{V}, \qquad [4]$$

where: C_{liq} = volumetric concentration of liquid aerosol material (dimensionless) m_u = mass of uranine (g) ρ_u = density of uranine (g/cm^3) = 1.53 g/cm^3 m_o = mass of oleic acid (g) ρ_o = density of oleic acid (g/cm^3) = 0.8935 g/cm^3 V = volume of the solution container (mL). For all liquid aerosols, 0.10 g uranine was mixed with each mL of oleic acid.

For solid aerosols, fluorescein (CAS 2321-07-05) was combined with ammonium hydroxide to form ammonium fluorescein. In order to ensure that all of the fluorescein was converted to ammonium fluorescein, the volume of ammonium hydroxide used was three times the stoichiometrically-calculated requirement to form ammonium fluorescein. Ammonium fluorescein was then mixed with an appropriate volume of deionized (DI) water to produce the final solution. This solution forms solid, spherical beads after being aerosolized.

For solid particles,

$$C_{\text{solid}} = \frac{m_{af}}{(\rho_{af})(V)}, \qquad [5]$$

where: C_{solid} = volumetric concentration of solid aerosol material (dimensionless), m_{af} = mass of ammonium fluorescein (g), ρ_{af} = density of ammonium fluorescein (g/cm^3) = 1.35 g/cm^3, and V = final volume of solution, including

unreacted ammonium hydroxide and DI water (mL). All generated particles were spherical, so their aerodynamic diameters were determined as:

$$Dp_a = Dp_p \sqrt{\rho_p}, \quad [6]$$

where: Dp_a = aerodynamic particle diameter (μm) and ρ_p = particle density (g/cm^3).

For the sizes of particles analyzed, slip correction factors for physical and aerodynamic particle diameters were similar and were, therefore, ignored for determining the aerodynamic diameter for the present analysis. Particles passed through a Kr85 charge neutralizer (Aerosol Neutralizer 3054; TSI Inc., Shoreview, MN, USA) before entering the wind tunnel at Point 1 of Figure 2.

Aerosol Sampling

According to 40 CFR 53.42(a), a test sampler must block no more than 15% of the cross-sectional area of the wind tunnel test section. The blunt surface area of the SA246 PM_{10} inlet blocked approximately 13% of the sampling plane with both of the 4-inch panels installed. In order to stay below the 15% blockage criteria and overcome difficulties achieving spatial concentration uniformity when challenging the sampler with large particles, a collocated isokinetic and sampling inlet configuration was not used in the TAMU wind tunnel. A system denoted as "hot swapping" was used to reduce uncertainty in the inlet tests that may have been caused by a lack of spatial uniformity of particle concentration across the sampling plane. This process is described in 40 CFR 53.43(a)(2)(ix) through 53.43(a)(2)(xiv). In summary, an isokinetic inlet designed to sample at a constant flow rate of 114 Lpm was placed in the wind tunnel and then "swapped" with the candidate sampler inlet during testing so that the inlets of the isokinetic sampler and the sampler under evaluation were located in the same point in the sampling plane (Figure 4). The PM_{10} inlet and isokinetic samplers were placed in the wind tunnel, one after the other in an alternating fashion, until at least three samples collected with each inlet were collected for a given particle generation event. Temporal uniformity tests were conducted that showed extremely low variation between concentrations measured consecutively with the isokinetic nozzles. Temporal uniformity was routinely checked with each particle size at which sampler performance was evaluated. If the coefficient of variation (COV) of raw concentrations (measured in FIU-g) for any given particle size exceeded 20%, data were disregarded. Most raw concentration data had COVs below 10%.

The isokinetic airflow was provided by a $^3/_4$ HP pump controlled by a valve. The flow rate was monitored using a HI-Q flow meter (D-AFC-09) that was calibrated by the manufacturer for the described application. The target set point for the pump was calculated using Equation (7):

$$Q_a = 44.1375 * \frac{P_a}{T}, \quad [7]$$

where: P_a = ambient pressure (mmHg), T = ambient temperature (K), and 44.139 = constant (aLpm-K/mm Hg) = 114 aLpm * 294.261 K/760 mm Hg.

The pump was allowed to warm up at the beginning of each day of testing and was then set to the appropriate flow rate at the beginning of each isokinetic test using the flow meter. At the end of each isokinetic test, the flow rate was again verified. The flow decreased with increasing test duration but never varied from the original setting by more than 10 Lpm and typically reached a minimum of approximately 106 Lpm.

Aerosol Size and Uniformity Measurements

Particle solutions were mixed to achieve a given particle size, but actual particle sizes and distribution were verified postgeneration. An Aerodynamic Particle Sizer (APS, Model 3321, TSI, Shoreview, MN, USA) was used to check if the particles were monodispersed, but the size reported by the APS was not used to indicate aerodynamic size because it is understood that stretching of liquid particles occurs during acceleration through the APS, biasing particle size measurements. Once the generated particles were deemed to be monodispersed, the particle stream was impacted onto slides coated with either an oleophobic solution (Nyebar - Type Q), for liquid particles, or Dow Corning high vacuum grease, for solid particles. The slides were then placed under a microscope with 400× magnification. A line slider was used to measure the apparent diameter (D_a) of impacted particles by counting the number of tick marks counted from one side of the particle to the other. The line slider was calibrated using a stage slide etched with lines spaced at 10 microns. Based on observations of particle size made using the APS before and after each test, aerosols were assumed to be monodisperse. As such, only 10–25 droplets were observed per particle size analyzed microscopically rather than the 100 required by 40 CFR 53.43(a)(2)(iv).

FIG. 4. Photos showing the (a) PM_{10} and (b) isokinetic inlet in the same sampling planes.

The spherical diameter (D_s) of droplets measured on the slides was determined using Equation (8):

$$D_s = \frac{D_a}{F}, \quad [8]$$

where F is the flattening coefficient. A flattening coefficient of 1.358 was used based on the use of Nyebar Type Q to treat slides and the uranine concentration of the particles (Faulkner and Haglund 2012).

Sampler Setup

The SA246 inlet was placed in the test section of the wind tunnel such that the sampling zone was located 0.305 m (half way) above the bottom of the wind tunnel (Figure 4). The filter cartridge, pump, and sampling lines were located below the wind tunnel. As previously noted, the PM_{10} sampler and isokinetic sampler were each placed in the wind tunnel, in an alternating sequence, to determine the sampling effectiveness of the PM_{10} inlet. A PQ200 flow control system (BGI, Inc.; Waltham, MA, USA) was used to control airflow through the sampler inlet at a flow rate of 16.7 L/min.

Filters are used to capture the particles sampled by isokinetic and PM_{10} inlets. A 47-mm diameter, PTFE, ring supported filters (P5PQ047, Pall Corporation, Port Washington, NY, USA) and 90 mm glass fiber filters (61664, Pall Corporation, Port Washington, NY, USA) were used to collect the particles sampled by the PM_{10} inlet and isokinetic samplers, respectively. The 47-mm filters were placed in a filter cartridge (F21, BGI, Inc. Waltham, MA, USA) and installed in the filter holder (F20, BGI, Inc. Waltham, MA, USA) that attaches to the base of the PM_{10} inlet. The 90-mm filters were placed directly into the isokinetic sampler and were held in place by the nozzle and knurled sleeve (Figure 5).

Inlet performance was assessed using a minimum of three pairs of isokinetic and PM_{10} inlet tests. An isokinetic sample was collected first, followed by a sample collected by the PM_{10} inlet. Test durations were developed based on experience and the need to meet the required signal to noise ratio of the measured fluorescence with a fluorometer (FM109515; Barnstead International; Dubuque, IA, USA). Run times were dependent on particle size and typically varied from 30 min to 6 h, with 12-h tests for large particles at a wind speed of 24 km/h. The relative error of all fluorometric precision measurements was less than 5%, as specified in 40 CFR 53.43(a)(2)(x).

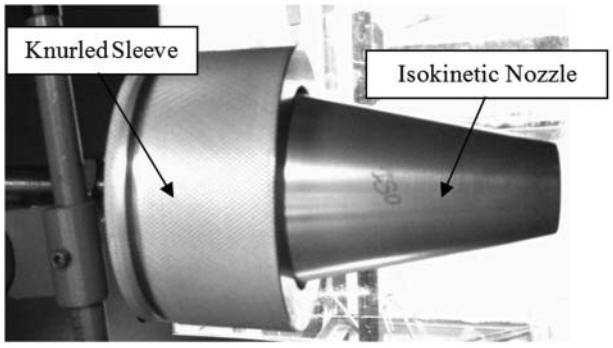

FIG. 5. An 8 km/h isokinetic nozzle.

Sample Analysis

After each inlet test, the sample filter was removed and placed into a measured mass of 0.01 N sodium hydroxide (for liquid particles) or 0.01 N ammonium hydroxide (for solid particles). For candidate inlet (47 mm) filters, approximately 10 mL of extractant was used while 30 mL of extractant was used for reference (90 mm) filters. Filters were soaked overnight and then analyzed with a fluorometer (FM109515; Barnstead International, Dubuque, IA, USA).

Signal Strength Considerations

An optical filter fluorometer was used to determine the relative fluorescent concentration of solutions in which fluorescently tagged particles collected on a sample filter were dissolved. The controls on filter fluorometers vary from manufacturer to manufacturer, but most include adjustment of photo multiplier tube (PMT) sensitivity, digital signal gain, and signal offset ("zero adjust"). Many fluorometers have special modes or software that allows signal intensity to be correlated with solution standards for direct measurement of concentration. In aerosol inlet studies it is not usually necessary to measure absolute concentration of the fluorescent tracer, but rather the relative concentration of fluorescein in the diluents for the candidate sampler and reference sampler filters. This mode is commonly known as "raw fluorescence" measurement.

Background signal may be detected by the fluorometer and may originate from fluorescence of the solvent, environmental fluorescent contamination, or from stray light reaching the PMT not associated with fluorescence of the sample. Such background signal does not originate from the tagged aerosol and must not be included in the sampler efficiency calculation. To eliminate background signal, most filter fluorometers have an offset control so that the signal can be "zeroed" using a blank (solvent only) solution. Once the fluorometer is "zeroed" the signal is considered to be solely attributable to the fluorescent tracer. This method of accounting for background fluorescent signal (i.e., "zeroing" the background signal by adjusting the fluorometer offset) was used in the original studies by McFarland and Ortiz (1984) when developing the original PM_{10} inlet (Carlos Ortiz, written personal communication, 14 August 2012).

Although "zeroing" of the fluorometer may simplify the analysis, it can mask significant errors when solution concentration is not sufficiently above the background signal. Since

the background level is not determined when the fluorometer is "zeroed," the threshold of detection cannot be known. In order to establish the threshold of detection, it is necessary to reduce the concentration of a solution containing fluorescent tracer using known dilution ratios. When the dilution ratio is known, the fluorescent signal of the diluted sample can be predicted from the product of fluorescent signal of the undiluted sample and the dilution ratio. For solutions having concentrations sufficiently above the background signal, the expected signal will vary linearly with concentration and will closely agree with the measured signal. As the solution concentration approaches the background signal, the expected signal will not equal the measured signal, indicating that the threshold of detection has been reached.

Figure 6 shows the relative error between expected and measured fluorometric concentration for serial dilution of a sample containing sodium fluorescein measured using the fluorometer employed in the present study. It can be seen that relative error remains less than 5%, as required by 40 CFR 53.43 (a)(2)(x), when the fluorescent concentration is at least 1.2× the background signal. When the fluorescent concentration is on the order of the background signal, the fluorometer signal becomes an unreliable indicator of solution concentration. Note that if the fluorometer were "zeroed," such breakdown would occur at a reading above "zero" (i.e., at a value of approximately 1.2× the unknown background), and the operator would have no indication that the signal reported by the fluorometer may be meaningless.

The existence of a lower threshold of detection of the fluorometer has implications for measurement of sampling efficiency, particularly when:

(1) Both the reference and candidate sampler filters have low concentration solutions (e.g., when sampling small test particles containing little fluorescent tracer mass), or

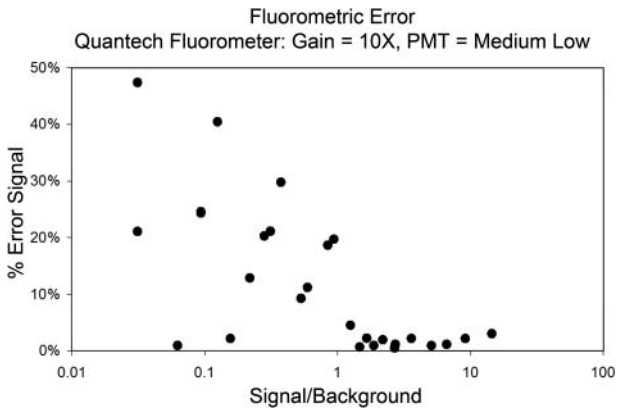

FIG. 6. Fluorometry error as a function of concentration signal-to-background signal ratio. The "signal" intensity was determined by subtracting the fluorometric intensity value of "blank" 0.01 N NaOH ("background" signal) from the measured intensity of 0.01 N NaOH containing known concentrations of fluorescein.

(2) The sampling efficiency of the candidate sampler being tested is low for a particle test aerosol size (e.g., when sampling 20 and 25 μm particles challenging a PM_{10} sampler).

In the first case, it is necessary to collect sufficient aerosol mass on the filters so that filter solutions will be well above the background level. In the second case, the reference filters may contain adequate concentration, but the sampler filter may not have meaningful concentration, and the efficiency value may not be determinable from the fluorometric data.

In the present study, rather than "zeroing" the offset of the fluorometer, the background signal was determined using a "blank" sample, and test durations were set to ensure that concentrations of fluorescein in analyzed aliquots were sufficient to yield a signal $\geq 1.2\times$ the background signal. In this manner, the relative error of concentration measurements on the extremes of the sampling efficiency curve (i.e., very small and very large particles) due to fluorometry was limited.

Given that the use of "offset adjustments" preferentially affects relatively large and small particles, this method of analyzing sampling efficiency values is expected to have trivial impact on results in the "sharp" portion of the sampling efficiency curve, near the cutpoint. As a result, sampling efficiency values around the cutpoint reported by McFarland and Ortiz (1984) and others employing this method of analysis are likely unaffected by fluorometry measurement errors arising from offset adjustments. However, small and large particle sampling efficiency values may be affected. It is unknown to the authors how VanOsdell and Chen (1990) and Tolocka et al. (2001) conducted fluorometric analysis of samples, but the fluorometric analysis methods employed by McFarland and Ortiz (1984) (i.e., use of "offset adjustments") may have biased analyses of sample specimens having low fluorometric signal, thereby artificially suppressing penetration values for large particles.

Sampling Effectiveness

The concentration of particles deposited on the PM_{10} inlet filter was determined using Equation (9):

$$C_{\text{inlet}} = \frac{\text{FIU}_{\text{inlet}} * m_{L,\text{inlet}}}{Q_{\text{inlet}}}, \quad [9]$$

where: C_{inlet} = calculated concentration of particles on PM_{10} inlet filter (FIU-g/Lpm), $\text{FIU}_{\text{inlet}}$ = average net fluorometric intensity of PM_{10} sample (FIU), $m_{L,\text{inlet}}$ = mass of liquid in which PM_{10} filter was soaked (g), and Q_{inlet} = flow rate through PM_{10} inlet (Lpm).

Because the isokinetic sampler design and flow rate combination were chosen in order to sample with an air velocity equivalent to the wind speed in the wind tunnel (i.e.,

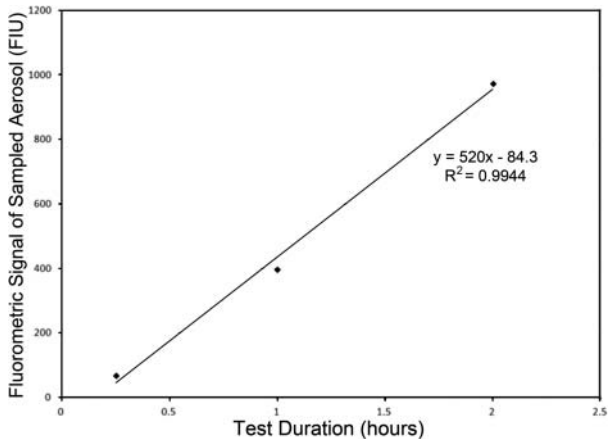

FIG. 7. Fluorometric intensity of sampled aerosol versus sampling time for isokinetic inlet.

isokinetically), the concentration of particles collected by the isokinetic sampler (adjusted for measured particle losses to the internal walls of the nozzle) is considered to be representative of the concentration of particles in the wind tunnel. As such the isokinetic sampler concentration was the reference concentration used for the evaluation of the PM_{10} inlet. Fluorometric intensity was linearly related to test duration ($R^2 > 0.99$; Figure 7) such that, for the isokinetic nozzle, a time ratio between the isokinetic sampler and PM_{10} inlet testing durations was applied to isokinetically measured reference concentrations (Equation (10)).

$$C_{\text{ref}} = \frac{\text{FIU}_{\text{iso}} * \ m_{L,\text{iso}}}{Q_{\text{iso}}} * \frac{t_{\text{inlet}}}{t_{\text{iso}}}, \qquad [10]$$

where: C_{ref} = reference concentration of particles based on isokinetic samples (FIU-g/Lpm), FIU_{iso} = average net fluorometric intensity of isokinetic sample (FIU), $m_{L,\text{iso}}$ = mass of liquid in which isokinetic filter was soaked (g), Q_{inlet} = flow rate through isokinetic inlet (Lpm), t_{inlet} = the testing duration for the PM_{10} inlet (h), and t_{iso} = the testing duration for the isokinetic sampler (h).

The inclusion of this time factor allows for shorter overall testing periods as the isokinetic testing times can be greatly reduced relative to the candidate inlet while still maintaining acceptable signal to noise ratios.

Background Signal Correction

An additional correction was made to both measured PM_{10} and reference concentrations to account for background fluorescent signal. Periodically, background control tests were conducted in which filters were placed in their respective samplers, which were installed in the wind tunnel as described, and the system was run for 30 min while the VOAG was not in operation. These filters were analyzed to determine the background signal generated by contamination of the wind tunnel, PM_{10} sampler, and isokinetic sampler. Similar tests in which filters were placed in their respective samplers and placed in the wind tunnel with no sample airflow yielded comparable background signals, indicating that background contamination was due to the filter handling process and was not the result of particles shearing from the wind tunnel surface. This result indicated that background concentrations observed should not be scaled based on the duration of a given test. Observed background signals were subtracted from the measured fluorometric concentrations to account for this background contamination before the effectiveness of the sampler for a given particle size was calculated. Failure to account for background signal may bias reported sampling effectiveness values either positively or negatively depending on the relative background values for both the isokinetic and candidate inlets.

RESULTS

Sampling Efficiency Versus Aerodynamic Particle Size

The performance of the PM_{10} inlet is described by the sampling effectiveness curve of the inlet, which relates sampling effectiveness to particle size. The sampling effectiveness curve for the SA246 PM_{10} inlet was constructed by plotting the fractional effectiveness of different particle sizes through the PM_{10} inlet. Data were collected for each particle size required by Subpart D (leftmost column of Table 3). Measured particle sizes reported are the result of microscopic measurements. The fractional effectiveness for each particle size was determined by dividing the concentration of particles collected by the PM_{10} inlet by the reference concentration from the isokinetic sampler (Equation (11)).

$$\text{Effectiveness} = \frac{C_{\text{inlet}}}{C_{\text{ref}}}. \qquad [11]$$

The sampling effectiveness for a given particle size was calculated for each pair of PM_{10} inlet-isokinetic datasets. The coefficient of variation (COV) for the sampling effectiveness at each size was calculated (Equation (12)).

$$\text{COV} = \sigma\bar{x}, \qquad [12]$$

where: σ = the sample standard deviation of the calculated sampling effectiveness, and $\bar{x}$ = the average calculated sampling effectiveness.

Measured sampling effectiveness values for particles with a nominal diameter of 3 μm exceeded 100%. Similar results were reported by VanOsdell and Chen (1990), with no reasonable explanation for why oversampling occurred. In the present work, and as reported by VanOsdell and Chen (1990), this change in the effectiveness value at 3 μm had no significant

TABLE 3
Sampling effectiveness results for SA246 PM_{10} sampler at 8 km/h

Required particle size (μm)	Particle size (μm)		Sampling effectiveness			
	Calculated[a]	Measured[b]	Not corrected[c,d]	Corrected[e]	COV (%)	Standard deviation
3 ± 0.5	3.01	3.03	1.152 ± 0.171	0.996	6.0	0.069
5 ± 0.5	5.22	5.20	0.916 ± 0.110	0.916	4.8	0.044
7 ± 0.5	7.22	7.50	0.759 ± 0.093	0.788	4.9	0.038
9 ± 0.5	8.82	8.90	0.591 ± 0.041	0.619	2.8	0.017
10 ± 0.5	10.38	9.80	0.596 ± 0.083	0.477	8.8	0.052
11 ± 0.5	10.63	10.72	0.403 ± 0.065	0.462	6.5	0.026
13 ± 1.0	13.14	12.79	0.272 ± 0.047	0.273	6.8	0.019
15 ± 1.0	14.10	14.50	0.191 ± 0.047	0.200	9.9	0.019
20 ± 1.0	19.71	20.00	0.034 ± 0.028[f]	0.057	33.2	0.011
25 ± 1.0	24.22 (liquid)	28.40	0.035 ± 0.008	0.035	8.9	0.003
	24.95 (solid)	25.51	0.032 ± 0.011[f]		14.3	0.005

[a]Calculated based on VOAG operating parameters and solution composition.
[b]Measured microscopically using flattening factor of 1.358 for liquid particles (Faulkner and Haglund 2012).
[c]Mean ±95% confidence interval.
[d]Measured sampling effectiveness, not corrected for multiplets and satellites.
[e]Corrected for multiplets and satellites.
[f]COV exceeds 10%.

impact on the predicted cutpoint of the sampler or the expected mass estimate for the SA246 inlet.

For testing as part of 40 CFR Part 53 Subpart D, the COV of sampling effectiveness values for each particle size must not exceed 10% (40 CFR 53.43(a)(2)(ix)). Data collected for nominal particle sizes of 20 and 25 μm did not meet these criteria. However, as indicated by the relatively low standard deviations of observed sampling effectiveness values, the large COVs resulted from dividing a relatively tightly grouped set of data by a small average effectiveness. The small standard deviations for these values indicate that the measured effectiveness values are consistent and credible. For particles in the 24–25 μm size range, there was no statistical difference in the measured sampler effectiveness for solid and liquid test aerosols. Sampling effectiveness values for large, liquid particles sampled at several wind speeds are shown in Table 4. Sampling effectiveness values for particles with nominal diameters of 20 and 25 μm, observed using methods intended to improve confidence in large particle values, were somewhat higher than those reported by previous researchers (Table 4).

TABLE 4
Observed sampling effectiveness values for large particles versus thoracic particle penetration

	Sampling effectiveness					
	20 μm particles			25 μm particles		
	2 km/h	8 km/h	24 km/h	2 km/h	8 km/h	24 km/h
Present study[a]	$0.5 \pm 0.3\%$	$3.4 \pm 2.8\%$	$5.4 \pm 2.5\%$	$0.01 \pm 0.01\%$	$3.5 \pm 0.8\%$	$3.8 \pm 1.4\%$
McFarland and Ortiz (1984)[b]	0.1%	1.0%	0.9%	—	—	—
VanOsdell and Chen (1990)[b]	—	—	—	2.3%	0.3%	3.1%
VanOsdell (1991)	—	—	—	1.2%	—	4.6%
Tolocka et al. (2001)	0.0%	1.6%	0.0%	0.1%	0.2%	0.0%
	Thoracic particle penetration					
	20 μm particles			25 μm particles		
"Ideal" Sampler (40 CFR 53)	0.0%			0.0%		
ISO (1995)	5.9%			1.8%		

[a]Mean ± 95% confidence interval.
[b]Multiplet corrected values; all other averages reported are not multiplet corrected.

Curve Fit

The sampler performance curve at 8 km/h wind speed was determined by fitting both a lognormal and sigmoidal curve to the observed liquid aerosol sampling effectiveness data by minimizing the sum of squared error between the predicted effectiveness model and the data shown in Table 3 without multiplet correction. For each particle size, between 10 and 25 particles were analyzed microscopically, and for only two particle sizes were doublet droplets observed (three for 3 μm particles and one for 10 μm particles). Before fitting the curve, effectiveness values of 100% and 0% for particle sizes of 1 μm and 50 μm, respectively, were added to the observed data per the requirements of 40 CFR Part 53.43(a)(2)(xx)(A). Microsoft Excel® was used to fit both lognormal and sigmoidal curves to the data by minimizing the sum of square errors (SSE) between observed effectiveness values and the fitted curves (Equation (13)).

$$min(\mathrm{SSE}) = \left(\sum (E_i - \eta_{\mathrm{ex},i})^2 \right), \qquad [13]$$

where: E_i = measured sampling effectiveness for particle size i, and $\eta_{\mathrm{ex},i}$ = expected (i.e., modeled) sampling effectiveness for particle size i.

The lognormal function proved to fit the nonmultiplet corrected data most appropriately and resulted in a sampler cutpoint of 10.07 μm with a slope of 1.54. These data indicate compliance with the performance parameters for "50% cutpoint" and "Liquid particle sampling effectiveness" required in Table D-1 of Subpart D and agree with results from previous studies (McFarland and Ortiz 1984; VanOsdell and Chen 1990; Tolocka et al. 2001; Lee et al. 2013).

Multiplet correction as described by Haglund et al. (2002) was then applied to sampling effectiveness data. For each nominal particle size shown in Table 3, measurements of particle size collected with the APS were used to quantify the relative mass concentrations of satellites and multiplets. (The APS has a maximum particle detection size of 20 μm, so a single effectiveness value was used for the 25 μm data point.) A "particle size correction factor" (f) was calculated to correct APS-measured particle size data, which tend to be skewed negatively when measuring liquid droplets due to particle stretching during acceleration in the detection region (Equation (14)).

$$f = \frac{D_a}{D_{\mathrm{APS,VMD}}}, \qquad [14]$$

where: D_a = calculated aerodynamic diameter of "monodisperse" particles, and $D_{\mathrm{APS,VMD}}$ = volume mean diameter reported by the APS.

This particle size correction factor was then applied to all APS-reported particle sizes for a given test. The expected sampling efficiency for each test aerosol was then calculated (Equation (15)).

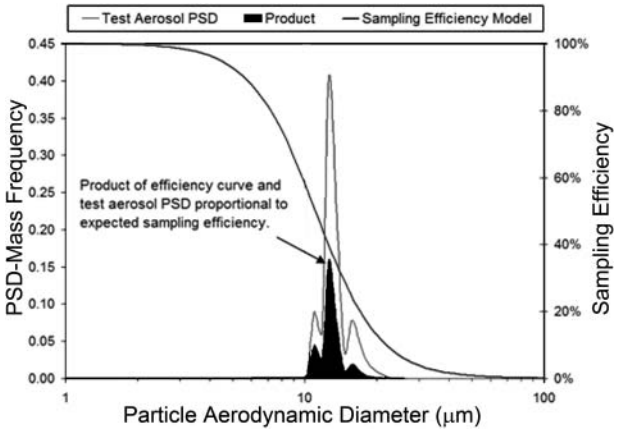

FIG. 8. Example of expected sampling efficiency for polydisperse test aerosol generated by a VOAG.

$$\eta_i = \int [\eta(d_p) \cdot f_{m,i}(d_p)] dd_p, \qquad [15]$$

where: η_i = expected sampling efficiency for test aerosol i, $\eta(d_p)$ = modeled sampling efficiency for particles of size d_p, and $f_{m,i}(d_p)$ = relative mass frequency of particles of size dp in test aerosol i.

Graphically, the expected sampling efficiency is represented by the area within the product of the sampling efficiency curve and the relative mass frequency distribution (Figure 8).

With the expected sampling efficiency for each test aerosol defined, the sampling efficiency model was fit to the experimental data using Microsoft Excel® to minimize the sum of square errors between observed effectiveness values and fitted curves (Equation (12)). An iterative process was used because each change in the sampling effectiveness model resulted in changes to the expected sampling efficiency for a given test aerosol (calculated using Equation (14)).

The best-fit lognormal curve for the multiplet correct data was characterized by a cutpoint of 10.18 μm with a slope of 1.52 (Figure 9). These data indicate compliance with the performance parameters for "50% cutpoint" and "Liquid particle sampling effectiveness" required in Table D-1 of Subpart D and little change from the nonmultiplet-corrected data.

Comparison to "Ideal Sampler" Performance

Based on the lognormal data fit, the expected mass concentration difference between the observed data and ideal sampler, including multiplet correction is 6.12%, indicating compliance with the performance parameter for "Liquid particle sampling effectiveness" required by Subpart D.

The nontrivial sampling of large particles by the FRM sampler is of little consequence in most urban environments,

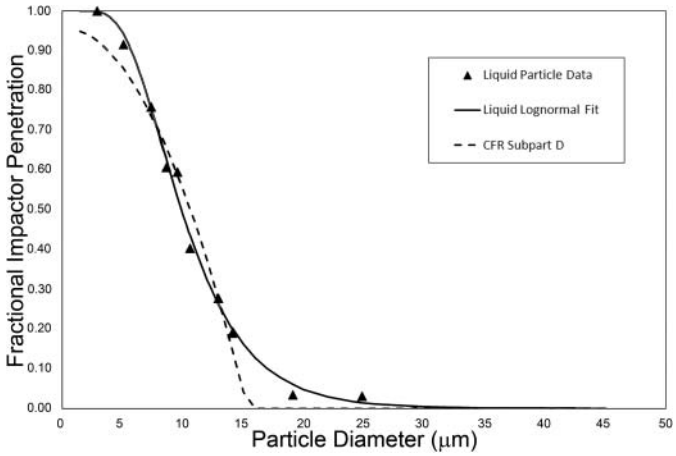

FIG. 9. Liquid particle effectiveness data at 8 km/h, lognormal performance curve with multiplet correction, and "ideal sampler" performance curve from 40 CFR Part 53 Table D-3).

where ambient aerosols are often characterized by relatively small particles. However, in rural environments where ambient aerosols are dominated by crustal particles, the median particle size is much larger (Table 1). A single 20-μm diameter particle of unit density will have a mass 1000× that of a 2-μm particle of equal density such that even relatively small sampling efficiencies of large particles can lead to nontrivial changes in measured concentrations of PM_{10}.

Figure 10 shows the relative concentration measured by the FRM sampler (with a sampling efficiency curve characterized by a cutpoint of 10.18 μm and a slope of 1.52) compared to the "ideal" PM_{10} sampler defined in Subpart D (dashed line in Figure 9) for a range of particle size distributions. These "sampling biases" are due to the "gap" between the sampler performance curve (solid line in Figure 9) and the "ideal sampler" curve for particles between ∼13 μm and ∼30 μm. Larger and more uniform aerosols have a greater fraction of their mass between these two size ranges, leading to these biases. "Oversampling rates" for the five PSDs shown in Table 1 are shown in Table 5.

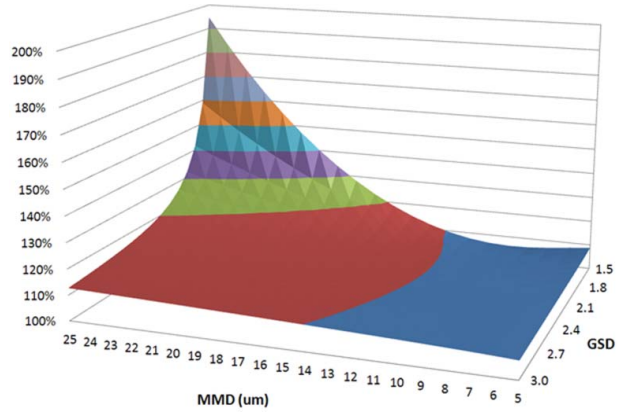

FIG. 10. Relative concentration measured by the FRM sampler (with a sampling efficiency curve characterized by a cutpoint of 10.18 μm and a slope of 1.52) compared to the "ideal" PM_{10} sampler defined in Subpart D.

TABLE 5
Relative concentration measured by FRM sampler compared to the "ideal" PM_{10} sampler and ISO 7708 (1995) thoracic fraction for aerosols described in Table 1

	Relative concentration	
Aerosol source	"Ideal" PM_{10} sampler[a]	ISO 7708 (1995)[b]
Urban[c]	103%	104%
Feedyard	115%	105%
Broiler housing	154%	98%
Dairy	112%	106%
Cotton gin	128%	101%

[a]Calculated as (Observed–Ideal)/(Ideal).
[b]Calculated as (Observed–ISO Value)/(ISO Value).
[c]Assumes uniform particle density for all three modes.

IMPLICATIONS

Two significant implications arise from the results of PM_{10} sampler performance tests for large particles:

(1) For sources of crustal PM such as agriculture and mining, then, the question of what fraction of PM penetrates the lung is non-trivial.

The sampling biases for large aerosols shown in Figure 10 can have significant implications for regulatory compliance in environments dominated by crustal particles. The FRM PM_{10} sampler measures higher concentrations downwind of sources than would the "ideal" sampler (as defined by Subpart D) that ostensibly mimics the penetration of particles in the human respiratory tract. If the Subpart D "ideal sampler" curve does mimic thoracic penetration, regulatory monitoring using FRM samplers would require more stringent controls on agricultural sources of PM_{10} than on urban sources with no requisite increase in protection of public health.

Such "oversampling bias" may contribute to the differences observed in PM exposure studies between health effects of urban aerosols versus crustal PM. (Differences in chemical composition likely contribute significantly to these differences as well.) Many of the epidemiological studies that have been used to set air quality standards have been conducted in urban settings, where populations are high enough to determine statistical differences in health effects, so "oversampling biases" were likely minimal. However, in rural settings, these biases are non-trivial.

(2) The current method of designating inlet performance for PM_{10} samplers is insufficient.

According to Subpart D, an inlet may be used as part of a FRM or FEM PM_{10} sampler if its performance in the presence of a single aerosol sufficiently approximates that of the "ideal" sampler. Based on the PSD of the aerosol specified in Subpart D, this criterion is relatively insensitive to penetration of large particles, which can have significant impacts in environments with a significant fraction of large particles.

A better approach would be to assess the performance of a candidate inlet against several aerosol PSDs that are representative of ambient PM found across the U.S. EPA has taken a similar approach in 40 CFR 53 Subpart F for $PM_{2.5}$ samplers, under which sampler performance is compared to an "ideal" sampler for coarse, "typical," and fine aerosol PSDs. In this manner, the sensitivity of inlets to large particles could be verified, significantly reducing or eliminating bias when measuring concentrations of large particulates.

CONCLUSIONS

The sampling effectiveness of a FRM PM_{10} inlet was evaluated in a wind tunnel using methods intended to reduce uncertainty in measured sampling effectiveness values of large particles. The results of the present sampler evaluation compared well with those of previous studies for a similar inlet near the cutpoint, and the sampler passed the criteria required for certification as a FRM sampler when tested at 8 km/h. Sampling effectiveness values for particles with nominal diameters of 20 and 25 μm exceeded 3% for 8 and 24 km/h wind speeds in the present study and were statistically higher than both the "ideal" PM_{10} sampler (as defined in 40 CFR 53) and the ISO (1995) standard definition of thoracic particles ($p < 0.05$) for 25 μm particles leading to the potential for significant sampling bias relative to the "ideal" PM_{10} sampler when measuring large aerosols.

REFERENCES

Berglund, R. N., and Liu, B. Y. H. (1973). Generation of Monodisperse Aerosol Standards. *Environ. Sci. Technol.*, 7(2):147–153.

Buser, M. D., Wanjura, J. D., Whitelock, D. P., Capareda, S. C., Shaw, B. W., and Lacey, R. E. (2008). Estimating FRM PM10 Sampler Performance Characteristics Using Particle Size Analysis and Collocated TSP and PM10 Samplers: Cotton Gins. *Trans. ASABE*, 51(2):695–702.

Capareda, S. C., Wang, L., Parnell Jr., C. B., and Shaw, B. W. (2004). Particle Size Distribution of Particulate Matter Emitted by Agricultural Operations: Impacts on FRM PM 10 and PM2.5 Concentration Measurements, in *Proc. of the 2004 Beltwide Cotton Production Conferences*, National Cotton Council, Memphis, Tenn.

Faulkner, W. B., and Haglund, J. S. (2012). Flattening Coefficients for Oleic Acid Droplets on Treated Glass Slides. *Aerosol Sci. Technol.*, 46:828–832.

Haglund, J. S., Chandra, S., and McFarland, A. R. (2002). Evaluation of a High Volume Aerosol Concentrator. *Aerosol Sci. Technol.*, 36(6):690–696.

International Standards Organization (ISO). (1995). *ISO 7708:1995(E): Air Quality: Particle Size Fraction Definitions for Health-related Sampling*. ISO, Geneve, Switzerland.

Lacey, R. E., Redwine, J. S., and Parnell Jr., C. B. (2003). Particulate Matter and Ammonia Emission Factors for Tunnel-Ventilated Broiler Production Houses in the Southern U.S. *Trans. ASAE*, 46(4): 1203–1214.

Lee, S., Yu, M., and Kim, H. H. (2013). Development of Aerosol Wind Tunnel and its Application for Evaluating the Performance of Ambient PM10 Inlets. *Atmos. Poll. Res.*, 4:323–328.

McFarland, A. R., and Ortiz, C. A. (1982). A 10 μm Cutpoint Ambient Aerosol Sampling Inlet. *Atmos. Environ.*, 16:2959–2965.

McFarland, A. R., and Ortiz, C. A. (1984). *Characterization of Sierra-Andersen PM-10 Inlet Model 246*. Air Quality Laboratory Report, Texas A&M University System, College Station, TX, 4716/02/02/84/ARM.

Tolocka, M. P., Peters, T. M., Vanderpool, R. W., Chen, F.-L., and Weiner, R. W. (2001). On the Modification of the Low Flow-Rate PM10 Dichotomous Sampler Inlet. *Aerosol Sci. Technol.*, 34:407–415.

United States Environmental Protection Agency (USEPA). (1996). *Air Quality Criteria for Particulate Matter*. Office of Research and Development, Washington, DC. EPA/600/P-95/001aF.

VanOsdell, D. W. (1991). *Wind Tunnel Test Report No. 29A: Test of the Rupprecht and Patashnick TEOM PM10 Sampler Inlet at 2 and 25 km/h*. Research Triangle Institute, Research Triangle Park, NC. EPA Contract 68-02-4550.

VanOsdell, D. W., and Chen, F. L. (1990). *Wind Tunnel Test Report No. 28: Test of the Sierra Andersen 246B Dichotomous Sampler Inlet*. United States Environmental Protection Agency. U.S. Government Printing Office, Washington, DC. EPA-68024550.

Wang, L., Parnell Jr., C. B., and Shaw, B. W. (2002). Performance Characteristics of Cyclones in Cotton-gin Dust Removal. *Agricultural Engineering - International: The CIGR Journal of Scientific Research and Development.* Manuscript BC 02 012. Vol. IV. August 2002.

Whitby, K. T., and Sverdup, G. M. (1980). California Aerosols: Their Physical and Chemical Characteristics. in *The Character and Origins of Smog Aerosols: A Digest of Results from the California Aerosol Characterization Experiment (ACHEX)*, G. M. Hidy, P. K. Mueller, D. Grosjean, B. R. Appel, and J. J. Wesolowski, eds., John Wiley & Sons, Inc., New York, NY, pp. 477–517.